Chemical Science

Accepted Manuscript

This article can be cited before page numbers have been issued, to do this please use: A. D'Souza, M. Mahajan and S. Bhattacharjya, *Chem. Sci.*, 2015, DOI: 10.1039/C5SC04108B.

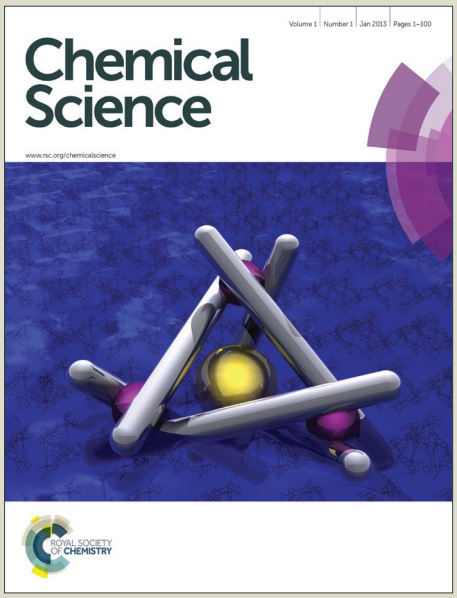

ROYAL SOCIETY OF CHEMISTRY

www.rsc.org/chemicalscience

ROYAL SOCIETY OF CHEMISTRY View Article Online
DOI: 10.1039/C5SC04108B

Chemical Science

EDGE ARTICLE

Designed Multi-stranded Heme Binding β-Sheet Peptides in Membrane

Received 00th January 20xx,
Accepted 00th January 20xx

DOI: 10.1039/x0xx00000x

www.rsc.org/

Areetha D'Souza, Mukesh Mahajan and Surajit Bhattacharjya[a]

Designed peptides demonstrating well-defined structures and functions in membrane environment are of significant interest in developing novel proteins for membrane active biological processes including enzymes, electron transfer, ion channel and energy conversion. Heme proteins' ability to carry out multiple functions in nature has inspired design of several helical heme binding peptides and proteins soluble in water and also recently in membrane. Naturally occurring β-sheet proteins, both water and membrane soluble, are known to bind heme, however, designing heme binding β-sheet proteins are yet to be reported, plausibly because of complex folding and difficulty in introducing heme binding sites in the β-sheet structures. Here, we describe design, NMR structures and biochemical functional characterization of four stranded and six stranded membrane soluble β-sheet peptides that bind heme and di-heme, respectively. The designed peptides contain either ^{D}P-G or ^{D}P-^{D}A residues for the nucleation of β-turns intended to stabilize multi-stranded β-sheet topologies and would ligate heme with bis-his coordination between the adjacent antiparallel β-strands. Further, we have optimized high affinity heme binding pocket, K_d ~ nM range, in the adjacent β-strands by utilizing a series of four stranded β-sheet peptides employing β- and ω-amino acids. We find that there has been a progressive increase in cofactor binding affinity in the designed peptides with the alkyl chain length of ω-amino acids. Notably, the six stranded β-sheet peptide binds two molecules of heme in a cooperative fashion. The designed peptides perform peroxidase activity with varying ability and efficiently carried out electron transfer with membrane associate protein cytochrome c. The current study demonstrated designing of functional β-sheet proteins in membrane environment and expands the repertoire of heme protein design.

Introduction

Designing synthetic proteins displaying structures and functions of naturally occurring proteins are of fundamental interest in chemistry and biology[1-6]. Because of the diverse functions of heme e.g. enzymatic, electron transfer and energy conservation, designing heme-proteins have drawn considerable attention in the past and present years[7-11]. It is mentioned worthy that heme containing enzyme cytochrome P450 is vital for metabolizing over 75% of the drugs in the current market[12-14]. Despite its high importance, lack of atomic-resolution structure of membrane anchored full length cytochrome P450 impedes in-depth understating of enzyme's catalytic power[12,13]. In particular, the structural plasticity of the catalytic site cytochrome P450 remains elusive[12-13]. Therefore, de novo designed heme binding peptides may be useful toward the plausible dissection of complex catalytic mechanism. In nature, helical as well as β-sheet proteins are known to bind heme to carry out biological functions (Fig. 1A). De novo designing of heme-proteins and metallo-proteins using helical structural scaffolds have been highly successful[7-11,15-17]. Recently, towards the design of functional membrane proteins, heme and metal binding helical proteins have been reported[18-22]. Heme binding to helical proteins has been mostly achieved by taking advantage of self-assembly of coiled-coiled structures. Whereby, either a single or multiple heme groups can be intercalated, through appropriately placed His residues, at the interface of coiled-coiled fold along the long axis of the helices (Fig. 1A). By contrast, self-assembly of β-sheets or β-strands may often lead to heterogeneous aggregations or amyloid formations[23-28]. The design of stable multi-stranded β-sheet structures or beta barrel structures soluble in membrane environment could be even more complex. Since, the stability and folding characteristics of β-sheet membrane proteins currently are not well understood[29-31]. Notably, de novo designed multi-stranded water soluble β-sheet proteins adopt open antiparallel β-sheet structures[32-35], with limited ligand binding sites. Particularly, design and characterization of atomic-resolution structures of β-sheet proteins that would bind to heme are yet to be reported. Beta barrel water soluble and membrane proteins are known to confer heme coordination[36,37]. A heme-iron transporter beta barrel membrane protein Has R with 22 antiparallel beta-strands binds heme at the surface of the barrel through bis-histidine coordination (Fig. 1A). In order to achieve heme binding β-sheet proteins, we have designed a series of

[a] School of Biological Sciences, 60 Nanyang Drive, Singapore, 637551, e-mail: surajit@ntu.edu.sg, Fax: +65-6791-3856
† Footnotes relating to the title and/or authors should appear here.
Electronic Supplementary Information (ESI) available: [details of any supplementary information available should be included here]. See DOI: 10.1039/x0xx00000x

peptides that would form well defined four stranded and six stranded β-sheet structures and display heme coordination at the targeted site with bis-histidine coordination. Designed peptides were solubilized, for functional and structural studies, in aqueous solutions containing dodecylphosphocholine providing a membrane mimic environment. Dodecylphosphocholine has been extensively used as a convenient detergent solution for reconstitution and NMR structure determination of membrane proteins including heme containing cytochromes[38-41]. Sequences of peptides-1 to peptide-7 are designed to adopt four stranded anti-parallel β-sheet structure where one heme cofactor is expected to be coordinated by two His residues between the β-strand 2 and β-strand 3. Peptide 8 has been designed to adopt six stranded β-sheet topology that would bind two molecules of heme, through bis-his coordination, between β-strand 2/β-strand 3 and β-strand 4/β-strand 5, respectively. Designed peptide sequences contain D-Pro-Gly residues for correct juxtaposition among the anti-parallel β-strands nucleating either type I′ or type II′ β-turn conformations[33,35]. Further, the designed sequences are rich in aromatic and hydrophobic amino acids with a propensity to form β-structures. It may be noted that a myristoylated N-terminus sequence (IFW^{D}PGHFV) used here for β-sheet design has been previously investigated showing β-hairpin structure and low affinity binding to heme[42].

Results and discussion

Topology and heme binding affinity of designed four stranded β-sheet peptides

Towards, the design of four stranded beta sheet peptides that would bind heme with high affinity at 1:1 stoichiometry, we first design and investigated peptide-1 (Fig. 1B). The primary structure of peptide-1 contains three ^{D}P-G sequences for juxtaposition of antiparallel β-strands in four stranded β-sheet structure. The ^{D}P9-G10 segment between the strand 2 and strand 3 would bring residues, H6, H13 in close proximity to confer heme ligation. We have utilized NMR spectroscopy to determine 3-D structures of the designed peptides. The secondary chemical shift of $^{\alpha}$H of each residue of peptide-1 delineated existence of four β-strands as revealed from positive deviation from random coil values (Supplementary Fig. 1). Residues ^{D}Pro-Gly showed negative deviation except for the residue ^{D}P9. NOESY spectra of peptide-1 revealed diagnostic long-range cross-strand NOEs establishing four β-sheet structure (Fig. 1C). An ensemble of 3-D structures of peptide-1, was obtained from medium and inter-strand long-range NOE-driven distance constraints (Fig. 1D and Supplementary Table 1). NMR structure of the designed peptide-1 is well defined with RMSD values for backbone (C^{α}, N, C′) atoms and all heavy atoms were estimated to be 0.30 Å and 0.57 Å, respectively (Supplementary Table 1). Supplementary Table 1 summarizes structural statistics of all the designed peptides. The four stranded β-sheet structure of peptide-1 is formed by strand 1: residues I1-W3, strand 2: residues H6-V8, strand 3: residues V11-H13 and strand 4: residues Y16-I18. The four stranded β-

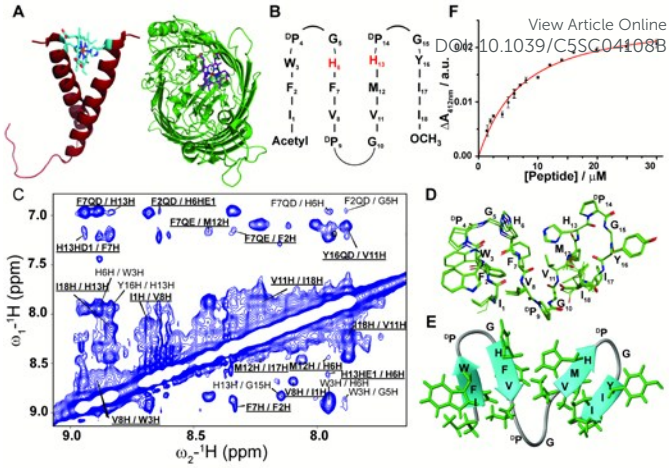

Figure 1: Design, structure and heme binding of four stranded β-sheet peptide-1. (A) Model helical peptide with heme (engineered glycophorin A) and β-barrel heme protein (PDB ID: 3CSN). (B) Design of peptide-1 with residues involved in heme ligation (red). (C) Section of two-dimensional ^{1}H-^{1}H NOESY spectra showing NOE connectivity between amide protons. Long range NOEs are underlined and boldfaced. (D) Superimposed twenty lowest energy structures of peptide-1. (E) Ribbon representation of peptide-1 structure with side chains. (F) Heme binding isotherm of peptide-1.

sheet topology of peptide-1 delineates close van der Waals packing interactions among sidechains of residues with neighboring β-strands (Figs. 1D and 1E). Notably, packing interactions can be realized between residues F2/F7 in strand1/strand2, residues M12/I17 in strand3/strand4 and residues V8/V11 in strand2/strand3 (Figs. 1D and 1E). Moreover, heme coordinating residues H6 and H13 of the peptide-1 are also found to be in close proximity (Figs. 1D and 1E). UV-vis spectroscopy experiments of titration of peptide-1 monitoring changes in Soret band of heme showed heme/peptide interactions (Supplementary Fig. 2A). Heme binding isotherm of peptide-1 has been analyzed following changes of heme absorbance at 412 nm (Fig. 1F). From the binding isotherm, peptide-1 binds to heme with an apparent dissociation constant (K_d) of 5.8±0.7 μM (Table 1). Bis-histidine-heme ligation of peptide-1 was supported by the red shift of the Soret band to 428 nm upon dithionite reduction (Supplementary Fig. 2B). Heme/peptide binding stoichiometry by Job's plot showed 2:1 peptide:heme (Supplementary Fig. 2C). Therefore, the data indicated that heme binding to peptide-1 plausibly requires a dimerization of the peptide in order to ligate one heme molecule through bis-histidine coordination. In other words, structure and heme binding of peptide-1 revealed that the four stranded β-sheet structure is achieved as per the design, however, high affinity heme binding targeted to the interface between strand 2 and strand 3 of the four stranded β-sheet structure has not been successful. We envision that low affinity heme binding and unexpected 2:1 stoichiometry observed for peptide-1 may be arising due to the lack of a binding pocket for heme between strand 2 and strand 3. Thus, residue ^{D}Pro9 deleted in peptide-2 may essentially diminish packing interactions between strand 2 and strand 3. However, peptide-2 also showed 2:1 (peptide:heme) stoichiometric ratio and an even lower K_d

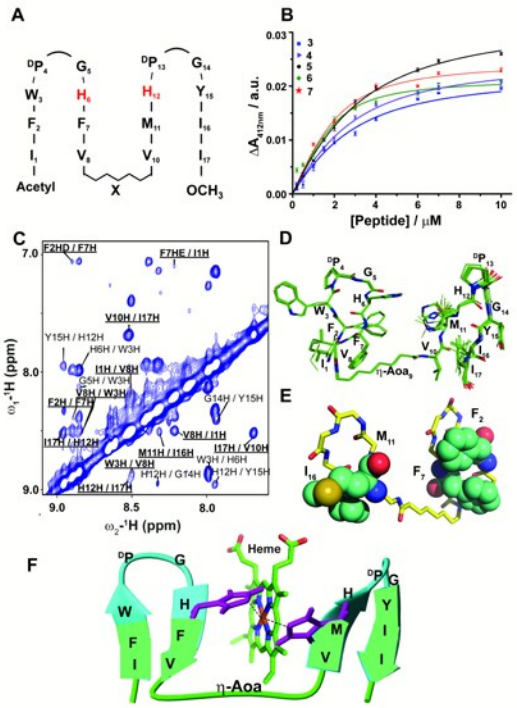

Figure 2: Design, structure and heme binding of four stranded β-sheet peptides. (A) Design of peptides 2-7 with His residues involved in heme ligation are shown in red. X_9 denotes Gly, βAla, δAva, εAca, ζAha and ηAoa in peptides 2,3,4,5,6 and 7, respectively. (B) Heme binding isotherms of peptides 3 (blue), 4 (purple), 5 (orange), 6 (green) and 7 (red). (C) Section of two-dimensional ^{1}H-^{1}H NOESY spectra showing NOE connectivity between amide protons. Long range NOEs are underlined and boldfaced. (D) Superimposed twenty lowest energy structures of peptide-7. (E) A selected structure of peptide-7 showing side chain packing within β-sheets. (F) Model structure of heme-peptide 7 complex. The side chains of the two axial ligands coordinating heme are shown (purple). Residues localized at the micelle/water interface (cyan) and residues localized in the hydrophobic core of micelles (green) are highlighted.

value of 8.9±0.9 μM for heme binding (Table 1). NMR analyses and atomic-resolution structure revealed that peptide-2 adopts a four stranded β-sheet structure with a hinge at residue G9, however, packing interactions between strand 2 and strand 3 have been highly diminished (Supplementary Fig. 3).

In order to create a high affinity heme binding pocket, we have replaced ^{D}P9-G10 sequence motif with amino acid β-Ala, in peptide-3. We assume that a higher degree of freedom at the Cβ-Cα bond of β-Ala[43-45] may allow one heme moiety to be coordinated with two His residues in the four stranded β-sheet scaffold. Interestingly, peptide-3 binds heme with significantly lowered K_d, 2.7±0.5 μM compared to peptide-1 and peptide-2 with expected stoichiometry of peptide:heme 1:1 ratio (Figs. 2A and 2B, Table 1, Supplementary Fig. 4). Bis-histidine heme coordination of peptide-3 has been confirmed by heme reduction upon addition of sodium dithionite (Supplementary Fig. 4). Secondary chemical shifts of $^{\alpha}$Hs showing positive deviation indicated four β-strands (Supplementary Fig. 5A) and further supported by several cross-strand NOEs for peptide-3 (Supplementary Fig. 5B). NMR structure revealed that four stranded β-sheet structures of peptide-3 with limited packing interactions between strand 2 and strand 3 (Supplementary Fig. 5C). The β-Ala residue assumed extended conformation and appears to be forming a short loop between strand 2 and strand 3 (Supplementary Fig. 5C). NMR structures of peptide-3 and peptide-2 demonstrated that heme coordinating His residues are not in close proximity in their apo-forms. However, it is likely loop flexibility conferred by the single methylene bridge between CH_2-CH_2 groups of β-Ala, compared to Gly, enables bis-histidine heme ligation with H6 (in strand 2) and H12 (in strand 3) of peptide-3. Encouraged by these observations, we further systematically investigated the length of the methylene units with heme binding affinity and stoichiometry. Designed peptides 4 to 7 contain increasing number of methylene units from δ-aminovaleric acid (three methylene groups) in peptide-4, ε-aminocaproic acid (four methylene groups) in peptide-5, ζ-aminoheptanoic acid (five methylene groups) in peptide-6, η-aminooctanoic acid (six methylene groups) in peptide-7. Heme binding studies of these peptides demonstrated that there has been a progressive increase in heme binding affinity with increase of the number of methylene units (Table 1). Heme binds to peptide-7 with the lowest K_d value of 400 nM, among the designed peptides, with 1:1 molar ratio (Fig. 2B, Supplementary Fig. 6). Secondary chemical shifts and NMR structures of peptides 4, 5 and 6 have been provided in Supplementary Figs. 7 and 8 establishing four stranded β-sheet topology.

Due to high affinity binding to heme, structure and micelle insertion of peptide-7 has been further carried out in more detail. CD spectroscopy has been used to determine global conformations of peptide 7 in apo and holo states (Supplementary Fig. 9). Peptide-7 showed an intense negative CD band at ~212 nm and relatively low intense positive CD band ~ 225-230 nm (Supplementary Fig. 9). These CD bands are diagnostic of β-sheet secondary structure containing exciton coupling arising from packing involving aromatic sidechains. CD spectra of peptide-7 in complex with heme demarcated discernable changes (Supplementary Fig. 9). As seen, the far UV CD band of the holo peptide-7 has been shifted from 212 nm (apo peptide) to 216 nm with a more intense band at 230 nm. These spectral changes might be reflecting towards an enhanced sidechain-sidechain packing interactions for the heme-bound peptide. Heme in complex with the designed peptide-7 showed an induced CD band at the Soret region of the absorption spectra, indicating that heme is experiencing a chiral environment in the holo state (Supplementary Fig. 9). Secondary chemical shifts of $^{\alpha}$Hs and inter-strand NOEs of peptide-7 identified segments of four β-strands and two β-turns for ^{D}P-G sequences (Supplementary Fig. 7). Fig. 2C shows a section of NOESY spectrum showing sequential and cross-strand backbone NH/NH NOEs of peptide-7. NMR structure of pepide-7 has been further refined using paramagnetic (PRE) NMR driven distance constraints since cross-strand NOEs were in paucity among residues of strand 2 and strand 3 limiting resolution of their spatial proximity in the structure. Residue H6 (in β-strand 2) of peptide-7 has been replaced by Cys and labelled with MTSL, a

Table 1: [a]Summary of heme binding affinity and enzymatic efficacy of the designed peptides

Peptide	K_d μM	k_{cat}/K_m 10^7 M^{-1} s^{-1}
1	5.8 ± 0.7	2.84
2	8.9 ± 0.9	2.91
3	2.7 ± 0.5	2.79
4	2.0 ± 0.2	2.44
5	1.6 ± 0.2	1.57
6	0.8 ± 0.2	1.34
7	0.4 ± 0.2	1.15
8	0.5 ± 0.1	4.35
9	28.1 ± 3.2	2.21
10	19.5 ± 2.1	1.30

[a] 9 and 10 represents peptide-8H6AH12A, peptide-8H15AH21A, respectively.

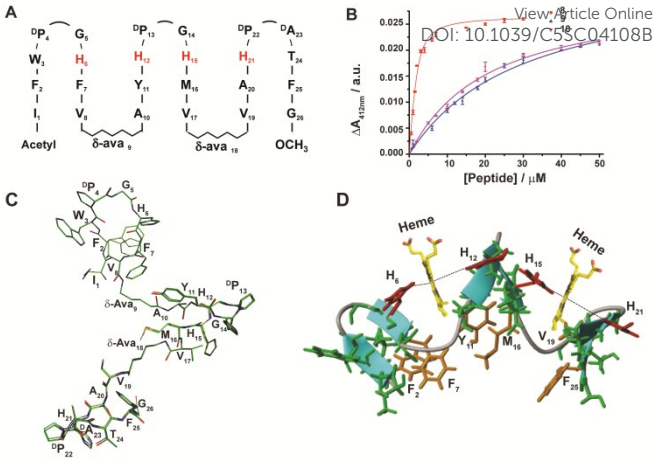

Figure 3: Design, structure and heme binding of six stranded β-sheet peptides. (A) Design of peptides 2-7 with His residues involved in heme ligation are shown in red. (B) Heme binding isotherms of peptide-8 (red), peptide-8H6AH12A or 9 (blue) and peptide-8H15AH21A or 10 (pink). (C) Superimposed ten lowest energy structures of peptide-8. (D) Model structure of heme-peptide-8 complex. The side chains of the four axial ligands coordinating heme are shown (red). Residues involved in side chain packing within β-sheets are highlighted (gold).

paramagnetic probe (on line methods) that would enhance relaxation of NMR active nuclei within 20 Å distance. The intensity changes of NH/C^{α}H cross-peaks observed in 2-D TOCSY spectra due to PRE effect were utilized as distance constraints for structure calculations for peptide-7 (Supplementary Table 1). The 3-D structure of peptide-7 reveals that strand 2 and strand 3 are orientated in a proximal fashion with a plausible binding pocket for heme insertion and ligation (Fig. 2D and 2E). Localization of peptide-7 into DPC micelles was investigated by PRE mediated resonance perturbation using spin labelled lipid 16-doxyl stearic acid (16-DSA). The PRE probe, 16-DSA would perturb resonances of amino acids located into the hydrophobic milieu of micelle, whereas residues at micelle/water interface would experience a lower degree of changes. 2-D TOCSY spectra of peptide-7 were obtained either in the absence of 16-DSA or in the presence of 16-DSA and backbone C^{α}H/NH cross-peak intensity changes were analyzed (Supplementary Fig. 10). Residues I1, F2, V8, η-aminooctanoic acid, V10, M11, Y15, I16 and I17 were significantly perturbed by inclusion of 16-DSA whereas residues of β-turns were less affected by the PRE probe (Fig. 2F, Supplementary Fig. 10). These observations indicated that hydrophobic residues in the four β-strands including η-aminooctanoic acid of peptide-7 are well inserted into non-polar milieu of micelles whereas residues in the β-turns including residues H6 and H12 are localized at the water/micelle. The surface localization of residues H6 and H12 provides coordination with the cofactor heme and may help in carrying out interfacial functions. 3-D structure of heme-peptide complex is yet to be available due to the unfavourable NMR spectra of heme-peptide complex resulting from high pH and high detergent concentrations required for NMR studies of heme-peptide complex. However, a molecular model of heme/peptide-7 complex (Fig. 2F) shows plausible mode of heme insertion at the binding pocket between strand 2 and strand 3 of peptide-7.

Topology and heme binding affinity of di-heme binding six stranded β-sheet peptides

We extended the design strategy to construct 26-residue six stranded β-sheet peptides that would ligate two molecules of heme employing residues H6/H12 at strand 2/strand 3 and residues H15/H21 at strand 4/strand 5, respectively (Fig. 3A). We have used δ-aminovaleric acid between strand 2 and strand 3 and strand 4 and strand 5 to accommodate two molecules of heme binding in the designed structure. Diagnostic inter-strand NOEs pertaining to β-sheet structure were detected for peptide-8 (Supplementary Fig. 11). An ensemble of structures of peptide-8 has been determined based on NOE-driven distance constraints (Fig. 3C, Supplementary Table 1). NMR structure of peptide-8 confirms six stranded β-sheet topology with loop conformations for δ-aminovaleric acid residues (Figs. 3 and 3d). The six stranded β-sheet structure of peptide-8 is typified by sidechain-sidechain packing among residues F2/F7, Y11/M16, V19/ and F25 (Fig. 3D). Heme binding of peptide-8 was estimated from spectral changes of the Soret band upon addition of peptide-8 (Supplementary Fig. 12A). Peptide-8 binds to heme at 2:1 (heme:peptide) stoichiometry as obtained from Job's plot (Supplementary Fig. 12B). Fig. 3E shows heme binding isotherm of peptide-8 delineating a sharp increase followed by saturation at higher concentrations of peptide-8. Binding isotherms revealed that peptide-8 binds heme with K_d of 0.5±0.1 μM (Table 1). Dithionite reduction of heme absorption spectra indicated bis-histidine coordination of peptide-8

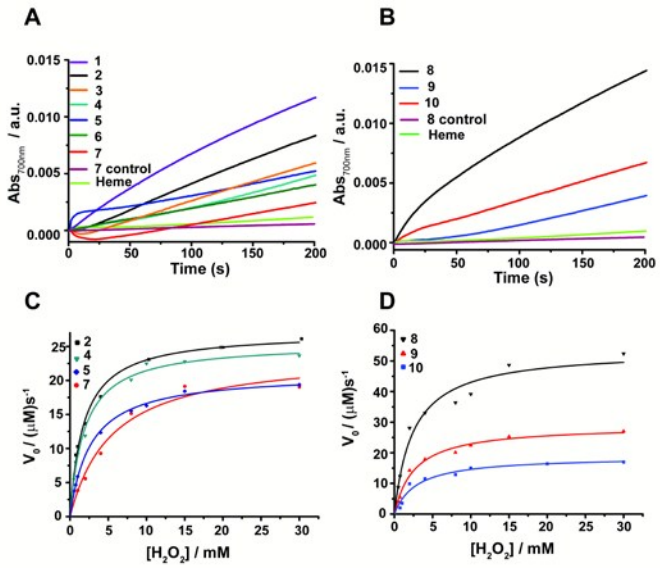

Figure 4: Peroxidase activity of designed β-sheet peptides. (A) Time course of ABTS oxidation at 700 nm for four stranded peptide-heme complexes at 4 mM H_2O_2 concentration. (B) Absorbance of ABTS oxidation at 700 nm versus time for six stranded peptide-heme complexes at 4mM H_2O_2 concentration. (C) Steady-state kinetics of ABTS oxidation as a function of hydrogen peroxide concentration for peptides 2,4,5 and 7. (D) Steady-state kinetics of ABTS oxidation as a function of hydrogen peroxide concentration for peptides 8, 9 and 10. In all cases, the final heme, peptide and ABTS concentration were 0.5μM, 4μM and 2.5mM respectively in sodium phosphate buffer, pH 7.2 containing 2mM DPC. The data was fitted to a Michaelis-Menten equation to derive catalytic parameters (Table1).

(Supplementary Fig. 12C). 3-D structure of peptide-8 in complex with two heme molecules has yet to be determined; however it is highly likely that binding of two heme molecules to the apo-peptide may cause a facile structural reengagement defining orientation of heme binding β-strands (Fig. 3F).

We note that peptide-8 demonstrated an appreciably lower K_d compared to peptide-4, four stranded β-sheet containing δ-aminovaleric acid (Table 1). Heme binding isotherm and lower K_d value of peptide-8 potentially indicated plausible cooperative heme interactions with the peptide-8. A dramatic decrease in heme binding affinity was observed for analogs of 8H15AH21A, binding heme between strand 2 and strand 3, displayed an appreciably higher K_d of 19.5 μM (Table 1). On the other hand, even a somewhat higher K_d value of 28 μM, was estimated for peptide-8H6AH12A (Table 1). These data indicated that two molecules of heme bind to peptide-8 in a highly cooperative manner, whereas ligation of a single heme is highly impaired. The origin of such cooperativity is likely to be involving rearrangement of β-strands at the heme binding pockets upon ligation of two heme moieties.

Peroxidase Activity of the designed β-sheet peptides

Peroxidase activity of heme bound peptides were examined using 2,2'-azino-bis(3-ethylbenzthiazoline-6-sulfonic acid) (ABTS), a substrate for peroxidase studies that undergoes a single-electron oxidation, as a reducing agent. Figs. 4A and 4B show time course of oxidation of ABTS in presence of H_2O_2 for four stranded β-sheet peptides (Fig. 4A) and for six stranded β-sheet peptide-8 and mutants in complex with heme (Fig. 4B). Enzymatic activity studies were also carried out for free peptides and also for free heme (Figs. 4A and 4B). These data suggest that peroxidase activity can be detected for heme-peptide complexes, although with different kinetics. The free heme or apo-peptides do not possess any enzymatic activity. Further, changes of the initial rates of product formation as a function of hydrogen peroxide concentrations for four stranded (Fig. 4C) and six stranded peptides (Fig. 4D) were estimated. Enzyme activity data were analyzed following Michaelis-Menten equation yielding k_{cat} and K_M parameters (Table 1). The catalytic efficiency, k_{cat}/K_M, among four stranded β-sheet peptides, peptide-1 to peptide-7, shows significant variation (Table 1). Peptide-2 demonstrated a high catalytic efficiency with k_{cat}/K_M of 2.91×10^7 $M^{-1}S^{-1}$, whereas catalytic efficiency of peptide-7 estimated to be the lowest with k_{cat}/K_M value of 1.15×10^7 $M^{-1}S^{-1}$ (Table 1). The peroxidase activity of the four stranded β-sheet peptides appears to follow an inverse correlation with their heme binding affinity. In other words, the tightest heme binding peptide-7 showed lowest catalytic activity whereas peptide-2 with lowest heme affinity delineated highest peroxidase activity (Table 1). As observed in heme-proteins, a tighter heme binding would confer a more rigid axial position of the porphyrin ring by coordinating histidine residue that reduces susceptibility to hydrogen peroxide[43,46]. Peroxidase activity of peptide-8, the six stranded β-sheet peptide, is remarkably high as compared to peptide-2 with k_{cat}/K_M of 4.35×10^7 $M^{-1}S^{-1}$ (Table 1). The superior peroxidase activity of peptide-8 may be attributed to the presence of two heme moieties involved in catalysis. The mutant peptides, peptide-8H15AH21A and peptide-8H6AH12A were appreciably less active compared to the parent peptide with lower k_{cat}/K_M values (Table 1). The catalytic efficiency of the mutant peptides appears to be comparable to four stranded β-sheet peptides binding to single heme. It may be noted that peroxidase activity of the designed peptides were significantly lower in comparison to the naturally occurring peroxidases[9,19,46] possibly due to hexa-coordinated states of the heme. Although, the designed peptides displayed peroxidase activity akin to previously reported designed heme proteins and peptides [9,19,46].

Electron transfer activity of peptide-7 and peptide-8 with cytochrome c

Heme containing proteins carry out electron transfer processes with other proteins in cell energy production. We investigated electron transfer activity of peptide-7 and peptide-8 with cytochrome c (cyt c), a small heme protein residing in the inner membrane space of mitochondria and known to be associated with lipids and micelles. Cyt c is a component of electron transfer chain in mitochondria required for the production of ATP. The heme group of cyt c performs electron transfer with membrane proteins bc1 complex and complex 4[47]. Fig. 5A compares UV-vis absorption spectra (500-650 nm) of heme in complex with peptide-7, cyt c in oxidized and also in reduced states and 2:1 mixture of peptide-7 (reduced) and cyt c (oxidized). The reduced heme, in peptide-

View Article Online
DOI: 10.1039/C5SC04108B

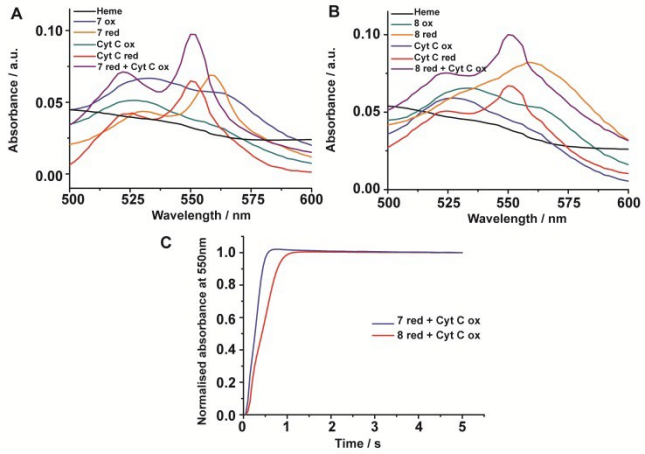

Figure 5: Electron transfer of four stranded and six stranded β-sheet peptides with CytC. (A) Absorption spectra of heme alone (black), peptide 7-heme: oxidized (blue), reduced (orange), Cyt C: oxidized (green), reduced (red) and 2:1 equivalent mixture of reduced peptide 7-heme and oxidized Cyt C (purple). (B) Absorption spectra of heme alone (black), peptide 8-heme: oxidized (green), reduced (orange), Cyt C: oxidized (blue), reduced (red) and 2:1 equivalent mixture of reduced peptide 8-heme and oxidized Cyt C (purple). (C) Absorbance monitored at 550nm versus time for reduced peptide7-heme/Cyt C oxidized (blue) and reduced peptide8-heme/Cyt C oxidized (red).The peptide/heme concentration was 24μM and Cytochrome c concentration was 12μM respectively.

7, showed two absorption peaks at 530 and 560 nm, whereas the reduced heme of cyt c displayed absorption peaks at difference positions at 520 and 550 nm (Fig. 5A). The absorption maxima of oxidized heme for both peptide-7 and cyt c were characterized by broad and unresolved peaks (Fig. 5A). Interestingly, the absorption spectra of heme in the mixture of reduced heme/peptide-7 complex and oxidized heme of cyt c revealed absorption spectra corresponding to reduced heme of cyt c (Fig. 5A). Similar observations can be made from the heme absorption spectra of peptide-8 and cyt c (Fig. 5B). These data clearly demonstrated that designed heme-peptides are able to undergo electron transfer function with a naturally occurring protein involved in the electron transport chain. The kinetics of electron transfer reactions were further examined for reduced heme-peptides, peptide-7 and peptide-8, and oxidized cyt c following changes in absorption at 550 nm wavelength (Fig. 5C). The rate constant of electron transfer has been found to be 2.28 s^{-1} and 1.6 s^{-1} for peptide-7 and peptide-8, respectively. Peptide-7, containing single heme, shows approximately 1.4 times faster electron transfer rate compared to di-heme binding peptide-8. It may be noted that electron transfer rate between cyt c and cytochrome c peroxidase has been estimated to be 0.23 s^{-1} [48]. These studies indicated that an efficient electron transfer occurs between peptide-7 and peptide-8 with cyt c.

Conclusions

Emulation of structures and functions of large proteins into small peptides is a challenging task. Unlike proteins, small peptides often lack defined folded structures and binding surface for interactions with ligands. Coiled coil helical peptides can self-assemble capturing heme within its binding interfaces. However, self-assembled β-sheet structures often generate insoluble fibrils or amyloids like materials. The present work demonstrates novel design principles for developing high affinity heme binding to well-defined multi-stranded β-sheet peptides. The introduction of beta and omega amino acids as loop residues in designing a high affinity heme binding pocket in β-sheet structures is critical. Designed peptides display enzymatic activity and facilitate electron transfer with a protein in electron transport chain in membrane mimetic environment. These structures and design can be further utilized to generate new classes of heme and/or metallo peptides and proteins functional in membrane and in solution. In addition, binding of heme to β-sheet structures has implications in understating mechanism of amyloids formation and neurotoxicity in Alzheimer's disease as heme/a-beta complex demonstrates peroxidase activity and has been linked to cellular neurotoxicity and aberrant neurotransmission[49]. Designing β-sheets/heme complexes would perhaps serve as model systems towards understating of the molecular mechanism of neurotoxicity of amyloids. Furthermore, autonomously folded synthetic β-sheet peptides in membrane environment may be exploited for destabilizing membrane protein/protein interactions for the development of novel therapeutics[50].

Materials and methods

Peptides and materials

Peptides were commercially synthesized from GL-Biochem (Shanghai, China). Crude peptides were subjected to purification by reverse phase HPLC Waters™ using C_4 column (300 Å pore size, 5 μM particle size). A linear gradient of acetonitrile/water (both solutions containing 0.1% v/v TFA) was used to elute the peptides while maintaining a constant flow rate of 2ml/min. The major sharp peak fraction obtained was then pooled and lyophilized. Masses of peptides were confirmed by mass spectrometry. DPC and deuterated compounds (DPC-d_{38}, D_2O) were purchased from Avanti polar lipids (Alabama, USA) and Cambridge Isotope Laboratories Inc. (Massachusetts, USA), respectively. 16-DSA was obtained from Sigma (St. Louis, MO, USA). 4, 4-dimethyl-4-silapentane-1-sulfonic acid (DSS) was acquired from Cambridge Isotope Laboratories, Inc. (Massachusetts, USA). Other chemicals including Sodium dithionite, Hemin, ABTS, and Cytochrome C were of analytical grade and purchased from Sigma-Aldrich.

Heme binding and Stoichiometric Analysis

The binding affinity of heme to designed peptides was characterized using a multi-well plate reader (Tecan Infinite M200 PRO) by titrating increasing concentrations of peptide (0-30μM) to a solution of 2μM heme prepared in 50mM sodium phosphate buffer, 2mM DPC, pH 7.2. The Soret band at 412 nm was monitored for complex formation for each aliquot after three hour incubation. Wavelength scans from 350-600 nm was further recorded to monitor the shift in the absorption maxima of heme on binding to the peptides. Binding isotherms were obtained by plotting the absorbance at 412 nm versus peptide concentration. The values of Δε and $K_{d,app}$ were derived from the ligand depletion binding model fit using Origin 9.0 [16, 51].

$$\Delta A_t = \frac{\Delta\varepsilon[([H_t] + [P_t] + K_{d,app}) - \sqrt{([H_t] + [P_t] + K_{d,app})^2 - 4[H_t][P_t]}}{2}$$

$[H_t]$ is the total heme concentration, $[P_t]$ is the total peptide concentration, $K_{d,app}$ is the apparent dissociation constant, Δε is the difference in extinction coefficients of bound and unbound heme , and ΔA_t is the change in absorbance for a fixed peptide concentration.

Peptide-heme stoichiometry was determined using method of continuous variation or Job's plot. 50μM peptide and heme stocks were prepared in 2mM DPC, 50mM sodium phosphate buffer, pH 7.2. Different ratios of the two stock solutions were mixed while keeping the total volume constant. The absorbance values at 412 and 356 nm were recorded for the various mole fractions of heme using a multi-well plate reader (Tecan Infinite M200 PRO). This difference in absorbance was then plotted against the mole fraction of heme.

Electron transfer experiment

Heme-peptide sample was prepared in 2mM DPC, 50mM sodium phosphate buffer pH 7.2 by incubating 24μM peptide to 24μM heme for 3 hrs. Reduced heme-peptide was prepared by addition of sodium dithionite to the heme-peptide sample. Cytochrome c of concentration 12μM was prepared using the identical buffer conditions. Absorbance scans were monitored from 350-600 nm in a multi-well plate reader (Tecan Infinite M200 PRO). The kinetics of the electron transfer reaction was followed spectrophotometrically at room temperature using a stopped-flow kinetics apparatus (SX20, Applied Photophysics). The rate constant for the reaction was determined by monitoring the changes in the absorption intensity at 550 nm versus time.

Enzymatic Assays

Peroxidase activity was evaluated in the presence of co-substrate, ABTS using a stopped-flow apparatus (SX20, Applied Photophysics). While one syringe was loaded with 8μM peptide, 1μM heme and 5.0mM ABTS mixture in 2mM DPC sodium phosphate buffer pH 7.2, the other syringe was loaded with hydrogen peroxide of required concentration in the identical buffer. The hydrogen peroxide stock solution concentration was standardized by UV–vis measurements (ε_{230} = 72.8 M^{-1} cm^{-1}). The reaction was initiated by injection of equal volumes from both syringes. The final heme, peptide, ABTS concentration were 0.5μM, 4μM and 2.5mM, respectively for each reaction. The steady-state kinetic parameters (K_m, V_{max}) in presence of ABTS were quantified by varying final concentrations of H_2O_2 from 0.5mM-30mM and monitoring the absorbance at 700nm. The absorbance at 700nm was further converted to concentration (ε_{700nm} =1.6 x 10^4 $M^{-1}cm^{-1}$). The reaction rates (V_0) for each H_2O_2 concentration were determined by linear regression analysis. The initial rates vs H_2O_2 concentration was plotted and fitted to the Michaelis-Menton equation using Origin 9.0 software.

$$V = \frac{V_{max}[H_2O_2]}{K_m + [H_2O_2]}$$

V is the reaction rate (μM/s), V_{max} is the maximal velocity for the enzymatic reaction (μM/s), K_m is the Michaelis-Menton constant and $[H_2O_2]$ is the concentration of H_2O_2 used. Turnover numbers (K_{cat}) were calculated by dividing the maximal velocity by the concentration of heme-peptide complex.

NMR and structural characterization

All NMR experiments were performed at 42°C on a Bruker DRX 600-MHz spectrometer equipped with a cryo-probe. NMR samples were prepared by dissolving the lyophilized peptide in 500μL 90% H_2O/10 % D_2O containing 125mM per-deuterated DPC. The concentration of the NMR sample was approximately 0.3-0.5mM. Two dimensional TOCSY (mixing time-80ms) and NOESY (mixing time-200ms) experiments were acquired for spin system assignments and structure determination. Chemical shifts of protons were internally referenced to 4, 4-dimethyl-4-silapentane-1-sulfonic acid (DSS). The proton resonances of all the amino acids were assigned unambiguously by overlaying TOCSY and NOESY spectrums and sequential walking. Backbone dihedral angles were then predicted after obtaining Hα, amide proton (and ^{13}Cα chemical shifts) of the assigned NOESY and 13C-1H HSQC spectra using PREDITOR. NOE restraints were derived from the NOE intensities of the assigned NOESY spectra and categorized into strong, medium and weak, respectively. This was further translated to distance limits between 2.5-5.0 Å. The NOE restraints and predicted dihedral angles values were used to carry out several rounds of structure calculations using CYANA 2.1. Of the 100 structures generated, 20 energy minimized structures were selected for evaluation and analyses. PROCHECK-NMR was used to assess the stereo-chemical

View Article Online DOI: 10.1039/C5SC04108D

quality of the structure ensembles. The structures are analyzed visually by PYMOL and MOLMOL.PRE experiments were carried out by titrating 2mM 16-doxyl-stearic acid (16-DSA) dissolved in deuterated methanol to a lyophilized peptide sample in DPC micelles. Two dimensional TOCSY spectra were carried out with and without the PRE probe using the same experimental conditions. The intensities of the CαH/NH cross peak were evaluated before and after the addition of the PRE probe and their ratio plotted for each amino acid. To facilitate MTSL (*S*-(1-oxyl-2,2,5,5-tetramethyl-2,5-dihydro-1H-pyrrol-3-yl)methyl methanesulfonothioate) labelling, peptide-7H6C was incubated with 10:1 MTSL:peptide concentration in 50% acetonitrile solution and incubated overnight at room temperature (>12 hours). In-order to remove excess MTSL and unlabelled peptide, the incubated sample was diluted and subjected to HPLC purification. The major eluted peaks were analyzed by mass spectrometry and the labeled peptide fraction was verified. The labeled peptide was then reconstituted in the same identical buffer conditions and two dimensional TOCSY spectra were carried out for the labelled and unlabelled peptide. The intensity of the TOCSY peaks observed for the labelled sample were used a measure to derive distance restraints for peptide-7 structure.

Acknowledgements

This work was supported by grants (RG 11/12, ARC 18/13) from the Ministry of Education (MOE), Singapore.

Notes and references

1 N. Koga, R. Tatsumi-Koga, G. Liu, R. Xiao, T. B. Acton, G. T. Montelione and D. Baker, *Nature*, 2012, **491**, 222-227.
2 Y. Mou, P.-S. Huang, F.-C. Hsu, S.-J. Huang and S. L. Mayo, *Proceedings of the National Academy of Sciences*, 2015, **112**, 10714-10719.
3 C. E. Tinberg, S. D. Khare, J. Dou, L. Doyle, J. W. Nelson, A. Schena, W. Jankowski, C. G. Kalodimos, K. Johnsson and B. L. Stoddard, *Nature*, 2013, **501**, 212-216.
4 A. J. Reig, M. M. Pires, R. A. Snyder, Y. Wu, H. Jo, D. W. Kulp, S. E. Butch, J. R. Calhoun, T. Szyperski and E. I. Solomon, *Nature chemistry*, 2012, **4**, 900-906.
5 S. Rajagopalan, C. Wang, K. Yu, A. P. Kuzin, F. Richter, S. Lew, A. E. Miklos, M. L. Matthews, J. Seetharaman and M. Su, *Nature chemical biology*, 2014, **10**, 386-391.
6 G. Kiss, N. Çelebi‐Ölçüm, R. Moretti, D. Baker and K. Houk, *Angewandte Chemie International Edition*, 2013, **52**, 5700-5725.
7 J. R. Anderson, C. T. Armstrong, G. Kodali, B. R. Lichtenstein, D. W. Watkins, J. A. Mancini, A. L. Boyle, T. A. Farid, M. P. Crump and C. C. Moser, *Chemical science (Royal Society of Chemistry: 2010)*, 2014, **5**, 507.
8 R. L. Koder, J. R. Anderson, L. A. Solomon, K. S. Reddy, C. C. Moser and P. L. Dutton, *Nature*, 2009, **458**, 305-309.
9 B. A. Smith and M. H. Hecht, *Current opinion in chemical biology*, 2011, **15**, 421-426.
10 M. Faiella, O. Maglio, F. Nastri, A. Lombardi, L. Lista, W. R. Hagen and V. Pavone, *Chemistry-A European Journal*, 2012, **18**, 15960-15971.
11 T. A. Farid, G. Kodali, L. A. Solomon, B. R. Lichtenstein, M. M. Sheehan, B. A. Fry, C. Bialas, N. M. Ennist, J. A. Siedlecki and Z. Zhao, *Nature chemical biology*, 2013, **9**, 826-833.
12 U. H. Dürr, L. Waskell and A. Ramamoorthy, *Biochimica et Biophysica Acta (BBA)-Biomembranes*, 2007, **1768**, 3235-3259.
13 I. G. Denisov, T. M. Makris, S. G. Sligar and I. Schlichting, *Chemical reviews*, 2005, **105**, 2253-2278.
14 Z. J. Wang, N. E. Peck, H. Renata and F. H. Arnold, *Chemical Science*, 2014, **5**, 598-601.
15 M. Faiella, C. Andreozzi, R. T. M. de Rosales, V. Pavone, O. Maglio, F. Nastri, W. F. DeGrado and A. Lombardi, *Nature chemical biology*, 2009, **5**, 882-884.
16 L. Di Costanzo, H. Wade, S. Geremia, L. Randaccio, V. Pavone, W. F. DeGrado and A. Lombardi, *Journal of the American Chemical Society*, 2001, **123**, 12749-12757.
17 M. Dürrenberger and T. R. Ward, *Current opinion in chemical biology*, 2014, **19**, 99-106.
18 B. M. Discher, D. Noy, J. Strzalka, S. Ye, C. C. Moser, J. D. Lear, J. K. Blasie and P. L. Dutton, *Biochemistry*, 2005, **44**, 12329-12343.
19 J. M. Cordova, P. L. Noack, S. A. Hilcove, J. D. Lear and G. Ghirlanda, *Journal of the American Chemical Society*, 2007, **129**, 512-518.
20 I. V. Korendovych, A. Senes, Y. H. Kim, J. D. Lear, H. C. Fry, M. J. Therien, J. K. Blasie, F. A. Walker and W. F. DeGrado, *Journal of the American Chemical Society*, 2010, **132**, 15516-15518.
21 M. Mahajan and S. Bhattacharjya, *ChemBioChem*, 2014, **15**, 1257-1262.
22 N. H. Joh, T. Wang, M. P. Bhate, R. Acharya, Y. Wu, M. Grabe, M. Hong, G. Grigoryan and W. F. DeGrado, *Science*, 2014, **346**, 1520-1524.
23 Ouberai, G. T. Dolphin, P. Dumy and J. Garcia, *Chemical Science*, 2011, **2**, 1293-1300.
24 J. S. Richardson and D. C. Richardson, *Proceedings of the National Academy of Sciences*, 2002, **99**, 2754-2759.
25 C. M. Rufo, Y. S. Moroz, O. V. Moroz, J. Stöhr, T. A. Smith, X. Hu, W. F. DeGrado and I. V. Korendovych, *Nature chemistry*, 2014, **6**, 303-309.
26 R. M. Hughes and M. L. Waters, *Current opinion in structural biology*, 2006, **16**, 514-524.
27 M. L. de la Paz, K. Goldie, J. Zurdo, E. Lacroix, C. M. Dobson, A. Hoenger and L. Serrano, *Proceedings of the National Academy of Sciences*, 2002, **99**, 16052-16057.
28 W. Wang and M. H. Hecht, *Proceedings of the National Academy of Sciences*, 2002, **99**, 2760-2765.
29 K. G. Fleming, *Annual review of biophysics*, 2014, **43**, 233-255.
30 S. H. White, *Nature*, 2009, **459**, 344-346.
31 L. K. Tamm, H. Hong and B. Liang, *Biochimica et Biophysica Acta (BBA)-Biomembranes*, 2004, **1666**, 250-263.
32 T. Kortemme, M. Ramírez-Alvarado and L. Serrano, *Science*, 1998, **281**, 253-256.
33 H. E. Stanger, F. A. Syud, J. F. Espinosa, I. Giriat, T. Muir and S. H. Gellman, *Proceedings of the National Academy of Sciences*, 2001, **98**, 12015-12020.
34 G. J. Sharman and M. S. Searle, *Journal of the American Chemical Society*, 1998, **120**, 5291-5300.
35 J. Venkatraman, S. C. Shankaramma and P. Balaram, *Chemical reviews*, 2001, **101**, 3131-3152.
36 M. Knipp and C. He, *Iubmb Life*, 2011, **63**, 304-312.
37 J. W. Fairman, N. Noinaj and S. K. Buchanan, *Current opinion in structural biology*, 2011, **21**, 523-531.
38 C. M. Franzin, P. Teriete and F. M. Marassi, *Journal of the American Chemical Society*, 2007, **129**, 8078-8079.
39 S. Ahuja, N. Jahr, S.-C. Im, S. Vivekanandan, N. Popovych, S. V. Le Clair, R. Huang, R. Soong, J. Xu and K. Yamamoto, Journal of Biological Chemistry, 2013, 288, 22080-22095.

40 M. Zhang, R. Huang, S.-C. Im, L. Waskell and A. Ramamoorthy, *Journal of Biological Chemistry*, 2015, **290**, 12705-12718.
41 M. Zhang, S. V. Le Clair, R. Huang, S. Ahuja, S.-C. Im, L. Waskell and A. Ramamoorthy, *Scientific reports*, 2015, **5**.
42 M. Mahajan and S. Bhattacharjya, *Angewandte Chemie*, 2013, **125**, 6558-6562.
43 S. Sakamoto, I. Obataya, A. Ueno and H. Mihara, *J. Chem. Soc., Perkin Trans. 2*, 1999, 2059-2069.
44 M. A. Molski, J. L. Goodman, F.-C. Chou, D. Baker, R. Das and A. Schepartz, *Chemical Science*, 2013, **4**, 319-324.
45 I. Karle, A. Pramanik, A. Banerjee, S. Bhattacharjya and P. Balaram, *Journal of the American Chemical Society*, 1997, **119**, 9087-9095.
46 S. Shinde, J. M. Cordova, B. W. Woodrum and G. Ghirlanda, *JBIC Journal of Biological Inorganic Chemistry*, 2012, **17**, 557-564.
47 R. Huang, M. Zhang, F. Rwere, L. Waskell and A. Ramamoorthy, *Journal of Biological Chemistry*, 2015, **290**, 4843-4855.
48 E. Cheung, K. Taylor, J. A. Kornblatt, A. M. English, G. McLendon and J. R. Miller, *Proceedings of the National Academy of Sciences*, 1986, **83**, 1330-1333.
49 H. Atamna and K. Boyle, *Proceedings of the National Academy of Sciences of the United States of America*, 2006, **103**, 3381-3386.
50 H. Yin, J. S. Slusky, B. W. Berger, R. S. Walters, G. Vilaire, R. I. Litvinov, J. D. Lear, G. A. Caputo, J. S. Bennett and W. F. DeGrado, *Science*, 2007, **315**, 1817-1822.
51 N. Gupta and S. W. Ragsdale, *Journal of Biological Chemistry*, 2011, **286**, 4392-4403.

View Article Online
DOI: 10.1039/C5SC04106B